EFFECTS OF AMBIPOLAR POTENTIAL ON MULTIPLE MIRROR CONFINEMENT

by

F. Najmabadi, A. J. Lichtenberg and M. A. Lieberman

Memorandum No. UCB/ERL M81/66

4 September 1981

ELECTRONICS RESEARCH LABORATORY

College of Engineering
University of California, Berkeley
94720

EFFECTS OF AMBIPOLAR POTENTIAL ON MULTIPLE MIRROR CONFINEMENT

F. Najmabadi, A. J. Lichtenberg, M. A. Lieberman

Department of Electrical Engineering and Computer Sciences
and the Electronics Research Laboratory
University of California, Berkeley, California 94720

ABSTRACT

The diffusion model for multiple mirror confinement has previously been limited to devices with a large number of cells and high mirror ratios. Ambipolar effects were assumed to reduce the confinement time by the usual factor $(1+Z\frac{T_e}{T_i})^{-1}$. For the ideal multiple mirror regime, in which the mean free path is shorter than the cell length but long compared to the mirror scale length, a new discrete stair-case density profile model, without those limitations, has been developed. A kinetic description for ion and electron transport in a multiple mirror device has been used. A self-consistent ambipolar potential is included. We have found that the ambipolar potential reduces the confinement time somewhat less than the usual ambipolar factor. Special attention is given to the last cell which acts as a boundary condition for our system. The ambipolar potential across the last mirror throat is studied and found to be of the order of $0.5kT_e$. For machines with small numbers of cells, significant improvements over previously calculated multiple mirror confinement times are found.

I. INTRODUCTION

Multiple mirrors are shown to be an effective way to reduce axial losses in open-ended devices. Various studies have shown that when the mean free path for 90° scattering, λ, is much smaller than the device length, L, imposition of additional mirrors over a simple mirror machine improves the confinement time substantially[1–5]. In this "multiple mirror" regime, mirrors act as fixed scattering centers; and particles, scattering between these centers, leave the system through a random walk process. This diffusive flow of particles results in a confinement time scaling as L^2.

Makhijani et al[1], using a computer code based on single particle motion, studied the scaling of the confinement time. They also developed a simple diffusion theory to study the confinement for the devices with large mirror ratios, $R \gg 1$, and sharp mirrors, $l_m \ll \lambda \ll l_c$, where l_m is the mirror scale length, $l_m \approx \left(\frac{1}{B}\frac{dB}{dz}\right)^{-1}$, and l_c is the cell length. In both calculations, they found $\tau_{mm} \sim L^2$. Experiments (Logan et al[2]) confirmed these scaling laws. Makhijani et al also found that the mean free path for scattering out of the loss cone angle θ_c, $\lambda^* \approx \lambda\theta_c^2 \approx \frac{\lambda}{R}$, separates two distinct regions in which the confinement time scales as L^2: 1) The ideal (high density) multiple mirror regime where $\frac{l_m}{R} \ll \frac{\lambda}{R} \ll l_c$, which has the maximum confinement time, and 2) The low density multiple mirror regime where $l_c \ll \frac{\lambda}{R} \ll L$. Using a kinetic description for ion and electron transport along a multiple mirror field, Mirnov and Ryutov[3] studied the low density multiple mirror regime. In their analysis, electron effects were included using a self-consistent ambipolar electric field. They found L^2 scaling for both heat and particle transport. In addition, their analysis showed that sharp mirrors ($l_m \ll l_c$) improve the confinement over a sinusoidal field variations.

Multiple mirror devices do not always operate in the ideal multiple mirror regime, such as during the start-up of a fusion device when plasma is cold and highly collisional, $\lambda \ll l_m$.

Makhijani et al treated the ideal magnetohydrodynamics (MHD) regime in which $\frac{\lambda}{l_m} \rightarrow 0$. They found that the axial loss process is sonic flow and the confinement time scales linearly with the number of cell (or L). Mirnov and Ryutov considered the viscous fluid regime, where $\frac{\lambda}{l_m} \ll 1$ but not negligible, and found a diffusive loss process. Miller[4] applied a viscous fluid analysis to the ideal multiple mirror regime by limiting the classical viscosity for large λ, and found the same scaling laws. Bravenec et al[5], using viscous magnetohydrodynamics flow equations, investigated the confinement when $\frac{\lambda}{l_m} \leqslant 1$. Their equations allowed them to study the system over a wide range of parameters, covering both the dominantly flow regime ($\frac{\lambda}{l_m} \rightarrow 0$) and the dominantly diffusive regime. In addition, they found a stair-case density profile which is typical of multiple mirror devices.

In this paper, we use kinetic theory to study the confinement and density profile in the ideal multiple mirror regime ($l_m \ll \lambda \ll R l_c$). We use a long, thin approximation: parameters vary only in the z direction and therefore have only non-zero derivatives with respect to z. The distribution function of particles in velocity space is also assumed to be axisymmetric. We consider a symmetric multiple mirror device with $2N+1$ cells. A source introduces S particles per unit time in the central cell (S ions and ZS electrons, where Z is the atomic number of the ions). Because of the symmetry, we restrict our study to only one half of the machine: from the central cell (cell no. 1) to one end (cell no. $N+1$). We assume modest mirror ratios ($R \gtrsim 3$), and a modest number of cells ($N \gtrsim 5$). We also assume sharp mirrors ($l_m \ll l_c$); therefore, each cell can be divided into a highly collisional region (bulk of the cell) and a relatively short, collisionless, mirror region. Because $\lambda \ll R l_c$, any particle, detrapped in one cell, will be retrapped and confined in the adjacent cell. The distribution function in each cell, then, depends only on the parameters of the adjacent cell. Fig. 1 shows two adjacent cells: cell no. j and cell no. j+1. We denote points j and j+1 as the centers of the cells j and j+1 respectively,

while points A and B represent the beginning and the end of the mirror region joining the two cells; point M is located at the mirror throat.

Instead of solving Boltzmann's equation for the system, we use our assumptions to find the distribution functions at each point (section II). We then apply moments of Boltzmann's equation to the fully collisional region, while single particle motion is used to determine the parameters of the collisionless mirror region. The moments of Boltzmann's equation can be summarized in the following conservation laws:

1) Conservation of particle flux--continuity equation:

$$F_s \equiv A\int d^3\mathbf{v}\, v_z f_s = \frac{Ze}{|q_s|}\frac{S}{2} = const \tag{1a}$$

2) Conservation of energy flux--energy equation:

$$\Sigma_s m_s Q_s \equiv \Sigma_s m_s A\int d^3\mathbf{v}\, v_z v^2 f_s = const \tag{1b}$$

3) Conservation of momentum flux (z component)--momentum equation:

$$\Sigma_s m_s P_s \equiv \Sigma_s m_s A\int d^3\mathbf{v}\, v_z^2 f_s = const \tag{1c}$$

where s is the particle species, q_s is the particle charge, and A is the cell cross sectional area. It is important to note that the first two conservation laws are valid even across the mirror region, while the momentum equation is valid only where $\mathbf{B} = B_z\hat{z}$. Particles exchange momentum with the magnetic field in the mirror region which results in a net force on the mirror coils.

The confinement time in multiple mirror devices scales as v_s^{-1}, where v_s is the thermal velocity, $v_s = (\frac{2kT}{m})^{1/2}$. So electrons diffuse out of the system much faster than ions (by a factor of $(\frac{m_i}{m_e})^{1/2}$). Thus multiple mirror machines are basically ion confinement devices and electrons are confined electrostatically via an ambipolar potential, similar to a simple mirror

machine. Previous studies[1,4] in the ideal multiple mirror regime usually treated the effects of the ambipolar potential crudely. They assumed that ambipolar effects can be taken into account by using the familiar factor $(1+Z\frac{T_e}{T_i})$ derived in the diffusion theory. In this work, we use a self-consistent ambipolar potential. By assuming that the electron distribution is maxwellian (section III), we can relate the density and the ambipolar potential through the Boltzmann relation.

To solve our equations analytically, we use our basic assumptions to introduce certain approximations. We can then, determine the parameters of each cell in terms of the parameters of its adjacent cell (section IV). Special attention is given to the last cell which acts as a boundary condition for our system. The ambipolar potential near the last mirror throat is studied and found to be substantially different from that of a simple mirror machine (section V). No restriction has been imposed on mirror ratios in any cell. Engineering considerations can be used to adjust the mirror ratios and optimize the confinement. Such a scheme is discussed in section VI. A comparison of the results with the previous work on multiple mirror confinement is presented in section VII.

II. ION DISTRIBUTION

The confinement time in each cell is much larger than the relaxation time for particles because $\lambda << Rl_c$. Therefore, we can assume that the distribution functions at points j and j+1 are drifting maxwellians with parameters n_j and n_{j+1} (density), v_{dj} and v_{dj+1} (drift velocity), and T_j and T_{j+1} (temperature),

$$f(n_j, v_{dj}, T_j) = \frac{n_j}{\pi^{3/2} v_{sj}^3} e^{-\frac{v_\perp^2 + (v_z - v_{dj})^2}{v_{sj}^2}} \tag{2}$$

Using (2) for f, one can find F, Q, and P, given by (1), to be

$$\frac{S}{2} = F_j = A_j n_j V_{dj} v_{sj} \tag{3a}$$

$$Q_j = A_j n_j V_{dj} v_{sj}^3 (2.5 + V_{dj}^2) = F_j v_{sj}^2 (2.5 + V_{dj}^2) \tag{3b}$$

$$P_j = A_j n_j v_{sj}^2 (0.5 + V_{dj}^2) \tag{3c}$$

where $V_{dj} \equiv \frac{v_{dj}}{v_{sj}}$, and parameters of point j+1 can be found by exchanging j with j+1 in (3).

To find the distribution function at A, we assume that a drifting maxwellian, $f(n_a, V_{da}, T_a)$, moves towards the mirror throat at point A. Particles which are not in the loss cone (region R_2) are reflected back with $f(n_a, -V_{da}, T_a)$. Particles in the loss cone (region R_1) will pass through the mirror throat and reach point B (Fig. 2a). As before, a drifting maxwellian, $f(n_b, V_{db}, T_b)$, moves towards the mirror throat at point B. Trapped particles are reflected back with $f(n_b, -V_{db}, T_b)$ (Fig. 3a). Particles that are not trapped will pass through and reach point A. We will show later that $V_d \ll 1$ and n_j is very close to n_{j+1}; therefore, the distribution functions at A and B are very close to a maxwellian and are not very distorted.

The mirror region AB is collisionless; so the laws of single particle motion govern this region. Constants of motion are: 1) Total energy--$E = \frac{1}{2}mv^2 + q\Phi$, 2) Adiabatic invariant--$\mu = \frac{w_\perp}{B}$. We define normalized constants of motion as:

$$\epsilon = V^2 + \phi \tag{4a}$$

$$\mu = \frac{V_\perp^2}{b} \tag{4b}$$

where $\epsilon \equiv \frac{E}{kT}$, $\phi \equiv \frac{q\Phi}{kT}$, $b \equiv \frac{B}{kT}$, and $V \equiv \frac{v}{v_s}$. The distribution functions in terms of these constants of motion are then preserved in the mirror region AB.

It is more convenient to consider the distribution in (ϵ,μ) variables rather than $(v_\perp, v_z)$ variables. The differential volume element at any point z transforms as

$$d^3v = 2\pi v_s^3 V_\perp \, dV_\perp dV_z = \pm \frac{\pi}{2} v_s^3 b_z (\epsilon - \phi_z - \mu b_z)^{-1/2} d\epsilon \, d\mu \tag{5}$$

where + (-) sign is used when $V_z > 0$ ($V_z < 0$). To transform the velocity space into $\epsilon\,\mu$ space, we note that V_z should be real at any point z ($\epsilon - \phi_z - \mu b_z \geqslant 0$). In Fig. 2b, the region to the right of the line $\mu = \dfrac{\epsilon - \phi_A}{b_A}$ is allowed in cell j ($V_z^2 \geqslant 0$). Of this distribution, that to the right of the line $\mu = \dfrac{\epsilon - \phi_M}{b_M}$ has $V_z^2 > 0$ at the mirror throat (region R_1). These particles, therefore, are in the loss cone of cell j. The remainder of the distribution, region R_2, is reflected back by the mirror field. Fig. 3b is similarly constructed except that a new region, R_3, appears. Particles in this region pass the mirror throat, but cannot get to point A. These particles are reflected back by the ambipolar potential in the region AM ($\Phi_A - \Phi_M$).

Using (4) and (5), the integrals in (1) for points A and B can be evaluated in $\epsilon\,\mu$ space. One can easily show that the contributions of the trapped particles (region R_2) to the F and Q integrals cancel out. Furthermore, using the conservation of the magnetic flux

$$A_M = \frac{A_j}{R_j} = A_z \frac{B_z}{B_M} \tag{6}$$

one finds that the particle flux in the mirror region is conserved: $F_z = F_A = F_B$. However, to evaluate the momentum flux, P, and the density at any point in the mirror region, the integrations should be carried out over the entire allowed $\epsilon\,\mu$ space.

III. ELECTRON DISTRIBUTION

Basically, one can make the same arguments as in section II to find the electron distribution function at different points; however, by substituting (3a) in (1a) for any cell, we get

$$n_e V_{de} v_{se} = Z n_i V_{di} v_{si} = Z\frac{S}{2} \tag{7}$$

The charge neutrality condition, $n_e = Zn_i$, then, results in $V_{de} = V_{di}(\frac{m_e}{m_i})^{1/2} << V_{di}$. In section IV, we will show that $V_{di}<<1$; therefore, $V_{de}<< V_{di}<<1$, which suggests that it is a very good approximation to assume that the electron distribution is maxwellian and the electron loss rate is determined only by the ambipolar potential. This assumption, together with the charge neutrality condition, enables us to relate the potential and the ion density through the Boltzmann relation:

$$\phi_1-\phi_2 = \frac{Ze}{kT_i}(\Phi_1-\Phi_2) = Z\frac{T_e}{T_i} Ln\ (\frac{n_1}{n_2}) \tag{8}$$

We will show in section IV that changes in the ambiploar potential between the cells are small and most of the potential appear near the end of the device. Therefore, electrons move between the cells quite freely. This freedom of movement, together with the high electron thermal conductivity parallel to the field lines, holds the electron temperature constant throughout the machine.

IV. DENSITY PROFILE

Evaluation and substitution of the fluxes at points A, B, j, and j+1 in the conservation laws, (1), together with the Boltzmann relation, (8), result in a set of eight equations in nine unknowns: $n_j, V_{dj}, T_j, n_a, V_{da}, T_a, n_b, V_{db}$, and T_b. One of these equations, $F_A = F_B$, is trivial; so we need two more equations to complete our set. These are found from the viscous magnetohydrodynamics equations which describe the change in the ion temperature in each cell. As a good approximation, one can assume that the flow in each cell is isothermal: $T_j = T_a$ and $T_b = T_{j+1}$. Note that T_j is not necessarily equal to T_{j+1}: there can be a change in the ion temperature across the mirror region. Our set of equations is now complete. In principle, one is able to solve these equations exactly (numerically) and find the parameters of cell no. j

(n_j, V_{dj}, T_j) in terms of the parameters of cell no. j+1. Instead of doing this, we introduce the following approximations that simplify the equations considerably.

A. Approximations

1) Earlier work[1,2] has shown that $\frac{n_j - n_{j+1}}{n_j} \approx \frac{1}{N-j}$ and $n_j - n_{j+1} \sim \frac{SR}{A_j v_s}$. Using (3a), for modest R and N, we get $V_d \sim \frac{1}{RN} \ll 1$ and $\frac{n_j - n_{j+1}}{n_j} \sim RV_d \ll 1$. Therefore, V_d and $\frac{n_j - n_{j+1}}{n_j}$ are of the same order. One can easily show that the change in drift velocities in adjacent cells is second order in V_d, $V_{dj+1} - V_{dj} \sim RV_d^2$. To simplify the evaluation of the integrals in (1) for points A and B, we expand the distribution functions in terms of V_d and keep only the first order terms.

$$f(n, V_d, T, \phi, b) \approx (1+2V_z V_d) f(n, 0, T, \phi, b) = \frac{n}{\pi^{3/2} v_s^3} (1+2V_d \sqrt{\epsilon - \phi - \mu b}) e^{-(\epsilon - \phi)} \qquad (9)$$

where $f(n, 0, T, \phi, b)$ is a maxwellian distribution ($V_d = 0$).

2) By substituting (3b) in (1b), we get

$$2.5(T_1 - T_{N+1}) = T_{N+1} V_{dN+1}^2 - T_1 V_{d1}^2 \qquad (10)$$

So to second order in V_d, we have $T_1 = T_{N+1} = T_i$, i.e. the ion temperature is constant throughout the machine.

3) If one applies the Boltzmann relation, (8), to cells j and j+1, one can easily show that the change in the potential between adjacent cells is also first order in V_d, $\phi_A - \phi_B \sim Z\frac{T_e}{T_i} RV_d \ll 1$.

B. Simplified Conservation Laws

Using the approximations from part a, we drop the second order terms in (3) and

substitute the result in the conservation laws. Then we have:

$$F_j = F_A = F_B = F_{j+1} = \frac{S}{2} \tag{11a}$$

$$Q_A = Q_B = 2.5 v_s^2 F_A \tag{11b}$$

$$n_j(1+Z\frac{T_e}{T_i}) = \frac{P_A}{0.5 A_j v_s^2} + n_A Z\frac{T_e}{T_i} \tag{11c}$$

$$n_{j+1}(1+Z\frac{T_e}{T_i}) = \frac{P_B}{0.5 A_{j+1} v_s^2} + n_B Z\frac{T_e}{T_i} \tag{11d}$$

where the terms with $Z\frac{T_e}{T_i}$ are electron momentum flux terms, and the factor Z is the result of the charge neutrality condition. Electron terms in the energy equation drop out because electrons are maxwellian.

C. The Density Step, $\Delta n = n_j - n_{j+1}$

With the aid of the same set of approximations, all of the integrals in (1) for points A and B can be carried out easily by keeping only the first order terms. We subtract (11d) from (11c), substitute the flux terms, and eliminate n_a, n_b, V_{da}, V_{db}, and $\phi_A - \phi_B$ with the aid of (11a), (11b), and the Boltzmann relation[6]. We then have

$$n_j - n_{j+1} = \frac{2}{\sqrt{\pi}} \frac{S}{A_M v_s} \frac{(\mu_{cj}^3 + \mu_{cj+1}^3)(\mu_{cj} + \mu_{cj+1})}{(1-\mu_{cj}^3) R_j + (1-\mu_{cj+1}^3) R_{j+1}} (1-c_p) \frac{C_a}{1+Z\frac{T_e}{T_i}} \tag{12}$$

where C_a and c_p are defined below. Knowing the density in the last cell and the field geometry (μ_c's, where $\mu_c \equiv \cos\theta_c$), one can use (12) to find the density in each cell. The drift velocity in each cell, then, can be found from (3a). Equation (12) can also be used to find the confinement time for a multiple mirror device, or to define a local diffusion coefficient.

Before calculating these quantities, we discuss some of the important terms in (12). The term c_p is the result of the difference in the mirror ratios in the adjacent cells. c_p is usually very small ($\leqslant 10^{-2}$), and $c_p = 0$ for $\mu_{cj} = \mu_{cj+1}$. The last term, $\dfrac{C_a}{1+Z\dfrac{T_e}{T_i}}$, is due to ambipolar effects, and C_a has the form

$$C_a \equiv \frac{1+\left[1+k_1(\mu_{cj}+\mu_{cj+1})\right]Z\dfrac{T_e}{T_i}}{1+\left[1+k_2(\mu_{cj}+\mu_{cj+1})\right]Z\dfrac{T_e}{T_i}} \tag{13}$$

where k_1 and k_2 are complicated functions of μ_{cj} and μ_{cj+1}. Equation (13) shows that in the limiting case of $Z\dfrac{T_e}{T_i} \to 0$ (no ambipolar potential), $C_a = 1$ and the ambipolar factor goes to 1. Furthermore, when $\mu_{cj} = \mu_{cj+1} \to 0$ (a solenoid with no mirrors), $C_a = 1$ and the ambipolar factor, $C_a\left(1+Z\dfrac{T_e}{T_i}\right)^{-1}$, becomes the usual ambipolar factor $\left(1+Z\dfrac{T_e}{T_i}\right)^{-1}$, as expected. A numerical calculation, in Fig. 4, shows C_a as a function of μ_{cj}, μ_{cj+1}, and $Z\dfrac{T_e}{T_i}$. The solid lines give values of C_a for different $Z\dfrac{T_e}{T_i}$ when $\mu_{cj} = \mu_{cj+1}$. The dashed lines give C_a for $Z\dfrac{T_e}{T_i} = 1$ with $\mu_{cj} \neq \mu_{cj+1}$. Fig. 4 also shows that C_a increases slightly with the increase in mirror ratio or $Z\dfrac{T_e}{T_i}$. For the practical range of parameters, C_a is between 1.1 to 1.2.

D. Diffusion Coefficient and the Confinement Time

We define a local diffusion coefficient from the relation

$$\frac{S}{2} = -D(z)A(z)\,\frac{dn}{dz} \approx -D(z)A(z)\,\frac{\Delta n}{\Delta z} \tag{14}$$

In the limit of large N, we have

$$\frac{\Delta n}{\Delta z} \approx -\frac{n_j - n_{j+1}}{0.5(l_{cj}+l_{cj+1})} \approx -\frac{n_j - n_{j+1}}{l_c(z)} \tag{15}$$

Substituting for $n_j - n_{j+1}$ from (12) in (15) and using the result in (14), we find

$$D(z) = \frac{\sqrt{\pi}}{8}\, l_c(z) v_s\, \frac{1-\mu_c^3(z)}{\mu_c^4(z)}\, \frac{1+Z\frac{T_e}{T_i}}{C_a(z)} \tag{16}$$

where C_a is a function of μ_c and, therefore, is a function of z, and we have set $\mu_{cj} \approx \mu_{cj+1} \equiv \mu_c(z)$.

The confinement time , τ_{mm}, can be defined as

$$\tau_{mm} = \frac{A}{S}\left(l_{c1} n_1 + 2 \sum_{j=2}^{N+1} l_{cj} n_j \right) \tag{17}$$

In order to simplify our expressions, we assume to have constant mirror ratios throughout the machine, $\mu_{cj} = \mu_{cj+1} = \mu_c$ and therefore $A_j = A_{j+1} = A$. We also assume that the density in the last cell, n_{N+1}, is of the same order as the density jump, $\Delta n = n_j - n_{j+1}$, so that an explicit determination of the last cell density is not required. Then, $n_j \approx (N+2-j)\Delta n$ and substituting for Δn from (12), we have

$$\tau_{mm} = \frac{1}{\sqrt{\pi}}\, \frac{L^2}{\bar{l}_c v_s}\, \frac{\mu_c^4}{1-\mu_c^3}\, \frac{C_a}{1+Z\frac{T_e}{T_i}} \tag{18}$$

where $\bar{l}_c$ is the average cell length.

$$\bar{l}_c = \frac{l_{c1} n_1 + 2 \sum_{j=2}^{N+1} l_{cj} n_j}{n_1 + 2 \sum_{j=2}^{N+1} n_j} \tag{19}$$

Equations (16) and (18) show that the ambipolar potential increases the diffusion coefficient

(decreases the confinement time) by the factor , $C_a^{-1}(1+Z\frac{T_e}{T_i})$, which is somewhat less than $1+Z\frac{T_e}{T_i}$. In a multiple mirror device, the ambipolar potential is distributed throughout the machine; therefore, one expects the ambipolar effects to be similar to the familiar factor $1+Z\frac{T_e}{T_i}$. However, the ambipolar potential appears as potential jumps near each mirror throat. There, a combination of magnetic and electric fields affects the particle diffusion. The factor C_a is the result of the interaction of these fields near each mirror throat.

For comparison with the previous work, we find the confinement time in the absence of the ambipolar effects. We set $Z\frac{T_e}{T_i} = 0$ in (18) to get

$$\tau_{mm} = \frac{1}{\sqrt{\pi}} \frac{L^2}{\bar{l}_c v_s} \frac{\mu_c^4}{1-\mu_c^3} \tag{20}$$

Makhijani et al[1] found the confinement time to be

$$\tau_{mm}^{\cdot} = \frac{\sqrt{\pi}}{4} \frac{L^2}{l_c v_s} R \approx 0.443 \frac{L^2}{l_c v_s} R \tag{21}$$

The confinement time in the new model, (20), has the same scaling law, $\frac{L^2}{l_c v_s}$, as Makhijani's but different dependence on mirror ratio. Makhijani et al, in their theoretical model with constant mirror ratio and no ambipolar potential (section III, ref. 1), assumed large mirror ratio and argued that, as a result, they could set the drift velocities in the mirror region, V_{da} and V_{db}, equal to zero. They found that the particle and the energy fluxes in the mirror region are connected through, $\frac{1}{2} m Q_A = 2 T_a F_A$. Comparing that with (11b), they concluded that $T_a = 1.25\, T_j$: the ion temperature in the mirror region is 1.25 times the ion temperature in the cell, which cannot be justified in physical terms.

For large mirror ratios, when μ_c is close to 1, one can expand the mirror ratio function in (20) in terms of the small parameter $\epsilon = 1-\mu_c$; then a simple expression for the confinement time will be

$$\tau_{mm} \approx 0.376 \frac{L^2}{l_c v_s}(R-2) \tag{22}$$

Fig. 5 shows the two confinement times, (20) and (21). The dashed line in Fig. 5 represents this approximate expression. Fig. 5 also shows that $\tau_{mm} \rightarrow 0$ when $R \rightarrow 1$ in agreement with the viscous magnetohydrodynamics models for multiple mirror confinement. We find the density in the last cell, n_{N+1}, below, to complete our density profile calculations.

V. LAST CELL AND BOUNDARY CONDITION

As the boundary condition in the last cell, we assume that no ion enters the device through the ends: integrals containing $f(n_b, V_{db}, \phi, b)$ in (1) vanish. But, in the last mirror region, our approximation, $V_d \ll 1$, is not valid and the complete expressions for fluxes must be used to find the last cell parameters.

Evaluation and substitution of the flux terms in the conservation laws, (11), together with the Boltzmann relation, (8), result in a set of nonlinear equations which is solved numerically. The solution determines the drift velocity at any point in the last cell. Note that for this calculation we again drop quadratic terms in the drift velocity in the center of the last cell, V_{dN+1}. Fig. 6 shows values of V_{dN+1} for different values of μ_c and $Z\frac{T_e}{T_i}$. The density, then, can be found from (3a). The drift velocity in the last mirror throat, V_{dM}, is approximately constant, $V_{dM} \approx 0.7 \approx \frac{\sqrt{2}}{2}$ or $v_{dM} \approx (\frac{kT}{m})^{1/2}$.

As before, we have obtained the expected qualitative result that the ambipolar potential increases the drift velocities, and therefore, reduces the confinement time. But the rate of increase in the drift velocities is smaller than the usual factor $(1+Z\frac{T_e}{T_i})$.

Fig. 7 shows the potential drop, ($\Delta\Phi = \Phi_A - \Phi_M$), in the last mirror throat for different last cell mirror ratios and $Z\frac{T_e}{T_i}$. The potential drop is about 0.5 kT_e, in contrast to a simple mirror machine, in which the potential drop is typically in excess of 4 to 5 kT_e. The loss cone in a multiple mirror device is almost full, compared to a simple mirror machine which is almost empty. Therefore, the difference between the density in the mirror throat and in the cell is small. This leads to a relatively moderate potential drop at the last mirror throat in multiple mirror devices. Fig. 7 shows that the potential drop, $\Delta\Phi$, increases as the mirror ratio increases. A reduction in $Z\frac{T_e}{T_i}$ also increases $\Delta\Phi$. Any increase in the mirror ratio or any decrease in $Z\frac{T_e}{T_i}$ reduces the loss cone angle; therefore, for fixed n_A, the number of particles which reach the mirror throat, n_M, becomes smaller. Since $\Delta\Phi \sim Ln\ (\frac{n_A}{n_M})$, $\Delta\Phi$, will increase as Fig. 7 shows. Note that even though $\Delta\Phi$ increases when $Z\frac{T_e}{T_i}$ decreases, the potential which acts on the ions, $\phi_A - \phi_M = Z\frac{T_e}{T_i}\ Ln\ (\frac{n_A}{n_M})$, decreases resulting in an increase in the confinement time, as expected.

VI. OPTIMIZED MULTIPLE MIRROR CONFINEMENT

Equations (12) and (3a) determine the parameters of cell j (n_j, V_{dj}) in terms of the parameters of cell j+1. No restriction has been imposed on μ_c's in any cell. A reasonable way to adjust μ_{cj} is to keep β constant throughout the machine. Because the density drops as one moves towards the end of the machine, the pressure drops significantly. From an engineering point of view, one desires to have the magnetic field as small as possible, so one can adjust the field so that β remains constant in all cells. The magnetic field, therefore, decreases as one moves towards the end of the machine, as

$$\frac{B_j^2}{n_j} = const \tag{23}$$

For classical collisional scattering, $\lambda \sim \frac{T^2}{n}$, the decrease in density near the end of the machine results in much longer cells to keep the device in the right mean free path regime ($\lambda << Rl_c$). An increase in the mirror ratio in the last cells can partly compensate for this effect and keep the cell length reasonable. Engineering considerations set a practical limit for the maximum field. We, therefore, assume that the maximum field in the mirror throats is constant, $B_{\max} = const$, which, together with (23) gives

$$n_j R_j^2 = n_{j+1} R_{j+1}^2 = const \tag{24}$$

If we adjust the mirror ratios so that (24) is satisfied, the change in the mirror ratio in adjacent cells will be first order in V_d, $\frac{R_{j+1}-R_j}{R_{j+1}} \sim \frac{n_j - n_{j+1}}{n_j} \sim RV_d << 1$.

The parameters of the last cell found from Fig. 6 and (3a), together with (12) and (24), uniquely determine the parameters of a multiple mirror device. Table I shows the result of numerical computations for a 15 cell multiple mirror device with last cell mirror ratio of 8.6 ($\mu_c = 0.94$) and $Z\frac{T_e}{T_i} = 1$. Figs. 8a and 8b show the profiles of the density and the potential in the same machine, respectively. They show the stair-case profile which is typical of multiple mirror devices. Fig. 8c shows the drift velocities in the same machine.

VII. COMPARISON WITH PREVIOUS RESULTS

The new model is compared with the numerical computations of Makhijani et al[1]. To compare, we set $S = 5\times10^{23}$ ($particles/sec$), $A = 1$ (cm^2), $R = 5$ ($\mu_c = 0.894$), $T = 2.5$ Kev ($v_s = 4.8\times10^5$ (m/sec)), and $N = 3$ (7 cell device). We find central cell parameters: $n_1 = 2.125\times10^{13}$ (m^{-3}) and $v_{d1} = 1.13\times10^4$ (m/sec), in excellent agreement with his results $n_1 = 2\times10^{13}$ (m^{-3}) and $v_{d1} = 1.2\times10^4$ (m/sec).

Yang et al[7], using Makhijani's diffusion coefficient, found that the density profile in the system has the form of

$$n(z) = n_1(1- \frac{2z}{L'})^2 \tag{25}$$

where $n_1 \equiv n(0)$. As the boundary condition, he assumed that the density goes to zero at the end of the device, $n(L/2) = 0$, or $L' = L$. Fig. 9 shows a comparison between the stair-case model and Yang's for a seven cell machine. The dashed line represents Yang's model, not using his boundary condition, but instead by adjusting L' so that the profile has the same density at the center of cell no. 2 ($L' = 9.8$ while $L = 5.2$). Fig. 9 shows that this adjusted profile has almost the same density in the center of each cell as the stair-case model. Therefore, the boundary condition $n(L/2) = 0$ is not accurate for devices with a small number of cells. When N is not large, the new model predicts longer confinement times than the ones obtained from the diffusion theory. For example, by using the stair-case model in a reactor with 11 cells, we have found a decrease in length of about 30% from the length predicted by the diffusion model[8].

In addition to the improved confinement time for machines with a small number of cells, the new model is flexible and, therefore, more advantageous for reactor calculations. We have used this model in our parameter optimization of multiple mirror reactors[8]. The multiple mirror fusion device considered there consists of a central solenoid with length l_{c1} and multiple mirrors on both ends. We show there that the diffusion density profile, (25), indicates that $l_{c1} = \frac{L}{3}$ for the shortest reactor. The new model results in $l_{c1} \approx 0.3L$. Engineering considerations demand the fewest number of cells possible. Therefore the shortest reactor is not necessarily the optimum reactor. We have found that with an increase of about 10% in the reactor length (and $l_{c1} \approx 0.4L$), the number of cells can be reduced to half of the shortest reactor. The new stair-case model, with its flexibility to find the density profile for any number of cells, is an important tool for this type of reactor optimization calculations.

ACKNOWLEDGEMENTS

This work was supported by the Department of Energy Contract No. DE-ATOE-76ET53059.

FOOTNOTES

[1] A. Makhijani, A. J. Lichtenberg, M. A. Lieberman, and B. G. Logan, Phys. Fluids **17**, 1291 (1974).

[2] B. G. Logan, I. G. Brown, M. A. Lieberman, and A. J. Lichtenberg, Phys. Fluids **17**, 1302 (1974).

[3] V. V. Mirnov and D. D. Ryutov, Nucl. Fusion **12**, 627 (1972).

[4] G. Miller, Los Alamos National Laboratory Report No. LA-7580-MS, 1978.

[5] R. V. Bravenec, A. J. Lichtenberg, M. A. Lieberman, and H. L. Berk, Phys. Fluids **24**, 1320 (1981).

[6] For the details of the calculations, see F. Najmabadi, Ph.D. Thesis, University of California, Berkeley, (1981).

[7] S. T. Yang and M. A. Lieberman, Nucl. Fusion **17**, 4 (1977).

[8] F. Najmabadi, A. J. Lichtenberg, and M. A. Lieberman, *Parameter Optimization Of Multiple Mirror Reactors*, Bulletin of the APS **25**, 936 (1980), Submitted to Nuclear Fusion.

TABLE I. Parameters of a 15 cell multiple mirror machine ($N = 7$) with $R_{N+1} = 8.6$ ($\mu_{cN+1} = 0.94$) and $Z\frac{T_e}{T_i} = 1$.

cell no.	μ_c	R	$\frac{n}{n_{N+1}}$	$\frac{l_c}{l_{cN+1}}$	$\frac{A}{A_{N+1}}$
8	.940	8.59	1.	1.	1.
7	.922	6.68	1.65	.707	.777
6	.908	5.71	2.27	.561	.664
5	.897	5.09	2.84	.470	.593
4	.886	4.66	3.40	.407	.543
3	.877	4.34	3.92	.360	.505
2	.869	4.08	4.43	.324	.475
1	.861	3.87	4.92	.295	.451

LIST OF FIGURE CAPTIONS

Fig. 1. Parameters of two adjacent cells: cell no. j and cell no. j+1, a) potential, b) magnetic field, c) density.

Fig. 2. The loss cone for the ions moving to the right in cell no. j, a) Velocity space, b) $\epsilon\ \mu$ space.

Fig. 3. The loss cone for the ions moving to the left in cell no. j+1, a) Velocity space, b) $\epsilon\ \mu$ space.

Fig. 4. Ambipolar term, $C_a(\mu_{cj},\mu_{cj+1},Z\frac{T_e}{T_i})$ versus μ_{cj}. Solid lines: $\mu_{cj}=\mu_{cj+1}$ and different $Z\frac{T_e}{T_i}$. Dashed lines: $\mu_{cj}\neq\mu_{cj}$ and $Z\frac{T_e}{T_i}=1$.

Fig. 5. Confinement time, τ_{mm}, versus the mirror ratio, R. Dashed line represents the approximate formula, (22).

Fig. 6. Drift velocity in the last cell, V_{dN+1}, for different mirror ratios and $Z\frac{T_e}{T_i}$.

Fig. 7. Potential drop, $\Delta\Phi=\Phi_A-\Phi_M$, in the last mirror throat for different mirror ratios and $Z\frac{T_e}{T_i}$.

Fig. 8. Parameters of a typical multiple mirror device. a) density, b) potential, c) drift velocity. z axis not in scale.

Fig. 9. Comparison of the density profiles in a 7 cell machine, new stair-case model and Yang's model, with $(n(L/2)=0)$. Dashed line represents the diffusion profile, (25), adjusted to pass point A.

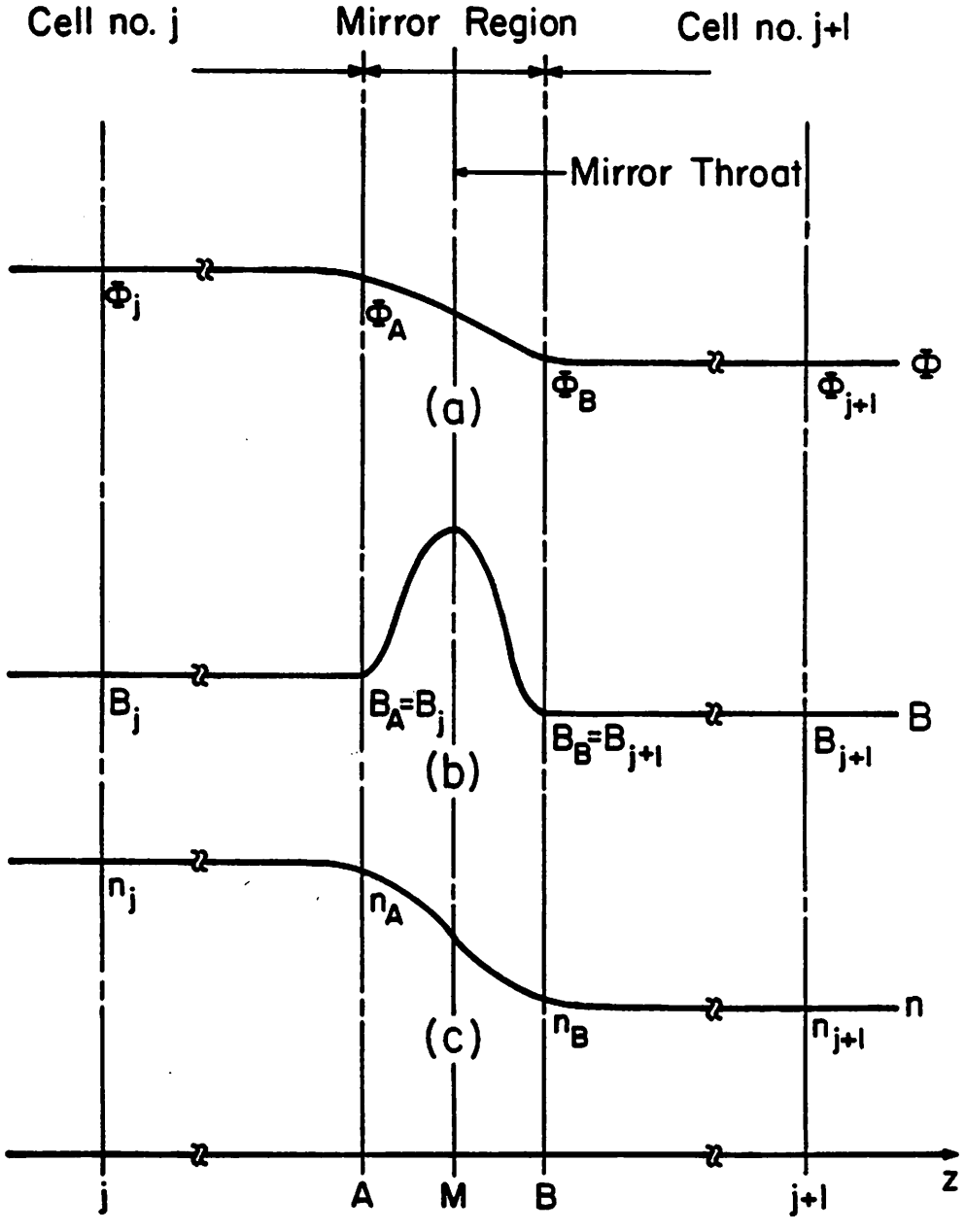
Cell no. j
Mirror Region
Cell no. j+l
Mirror Throat
Φ_j
Φ_A
Φ_B
Φ_{j+l}
Φ
(a)
B_j
$B_A=B_j$
$B_B=B_{j+l}$
B_{j+l}
B
(b)
n_j
n_A
n_B
n_{j+l}
n
(c)
j
A
M
B
j+l
z

Figure 1.

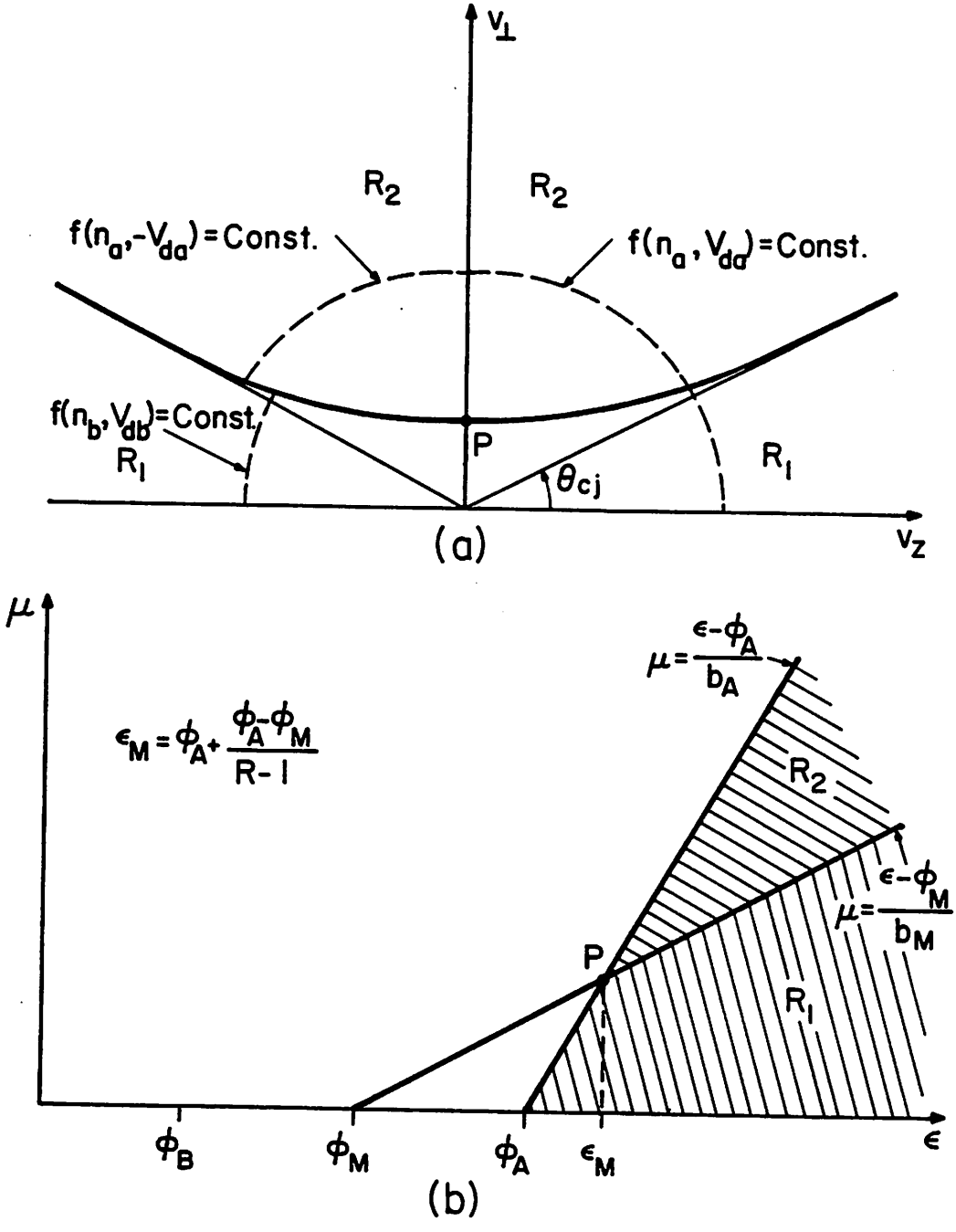
$v_\perp$
R_2
R_2
$f(n_a,-V_{da})=\text{Const.}$
$f(n_a,V_{da})=\text{Const.}$
$f(n_b,V_{db})=\text{Const.}$
R_1
P
θ_{cj}
R_1
v_z
(a)
μ
$\epsilon_M=\phi_A+\frac{\phi_A-\phi_M}{R-1}$
$\mu=\frac{\epsilon-\phi_A}{b_A}$
R_2
$\mu=\frac{\epsilon-\phi_M}{b_M}$
P
R_1
ϕ_B
ϕ_M
ϕ_A
ϵ_M
ϵ
(b)

Figure 2.

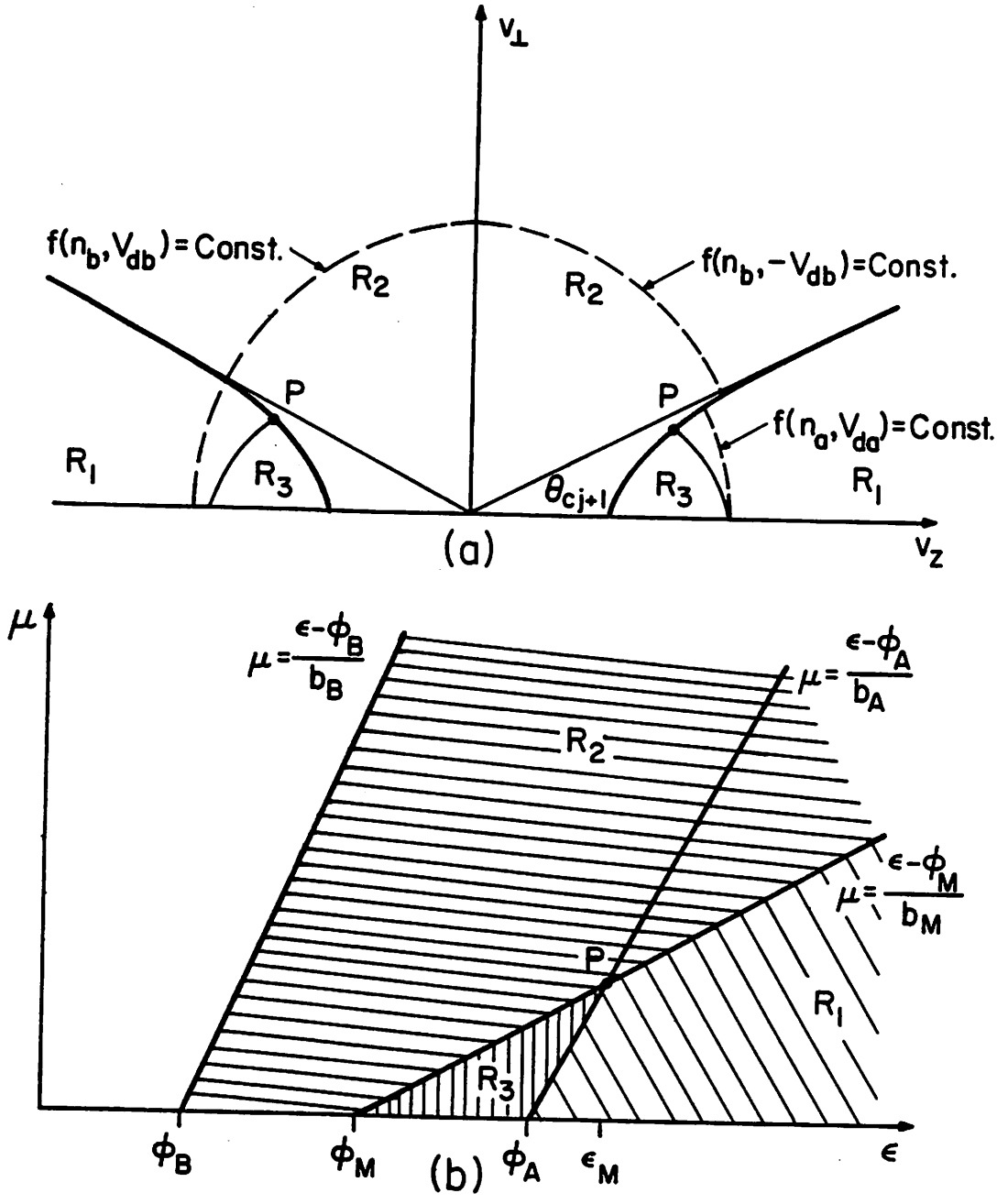
$v_\perp$
$f(n_b, V_{db}) = \text{Const.}$
$f(n_b, -V_{db}) = \text{Const.}$
$f(n_a, V_{da}) = \text{Const.}$
R_2
R_2
P
P
R_1
R_3
θ_{cj+1}
R_3
R_1
(a)
v_z
μ
$\mu = \frac{\epsilon - \phi_B}{b_B}$
$\mu = \frac{\epsilon - \phi_A}{b_A}$
R_2
$\mu = \frac{\epsilon - \phi_M}{b_M}$
P
R_1
R_3
ϕ_B
ϕ_M
(b)
ϕ_A
ϵ_M
ϵ

Figure 3.

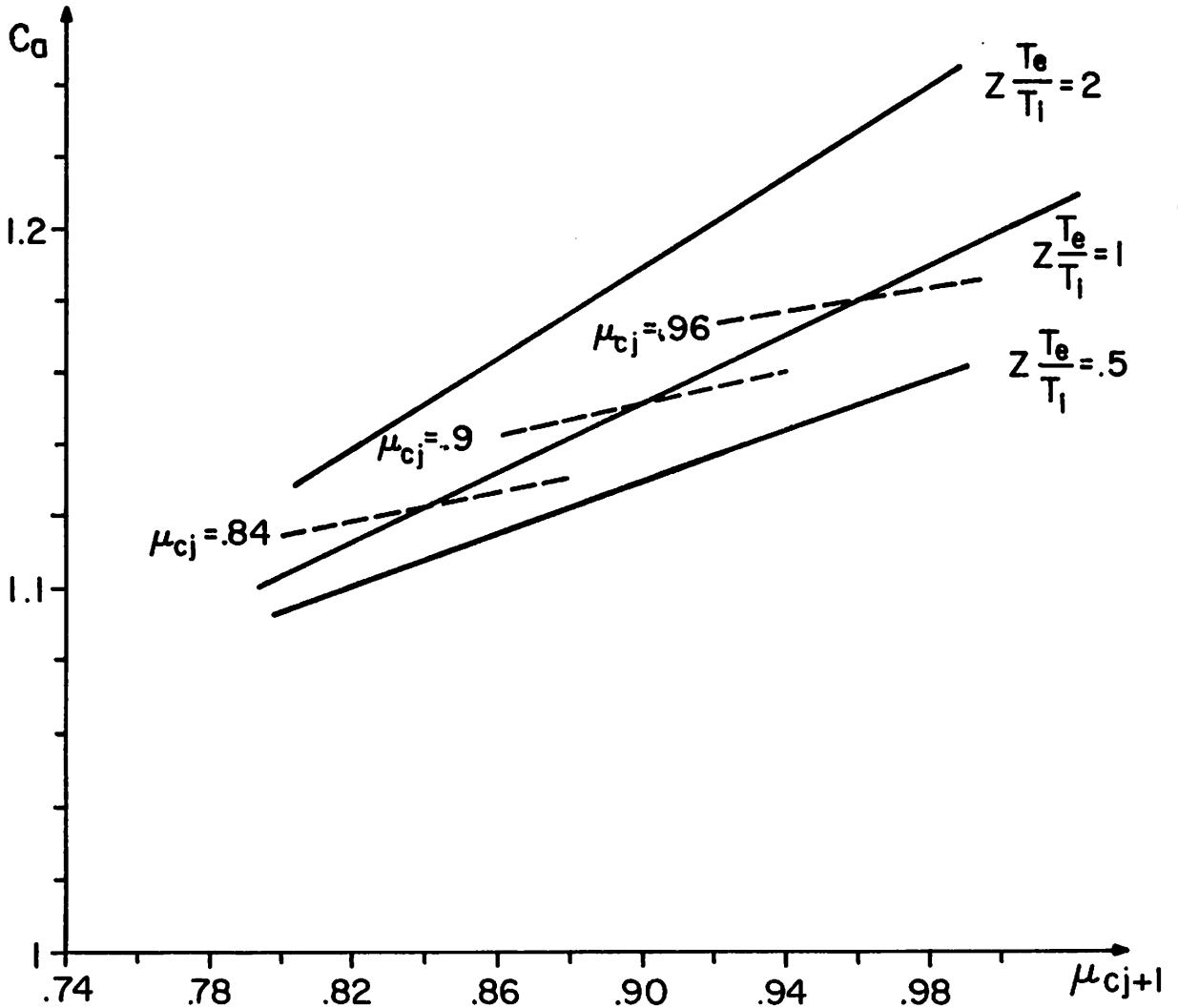
C_a
1.2
1.1
1
$Z\frac{T_e}{T_i}=2$
$Z\frac{T_e}{T_i}=1$
$Z\frac{T_e}{T_i}=.5$
$\mu_{cj}=.96$
$\mu_{cj}=.9$
$\mu_{cj}=.84$
.74
.78
.82
.86
.90
.94
.98
μ_{cj+1}

Figure 4.

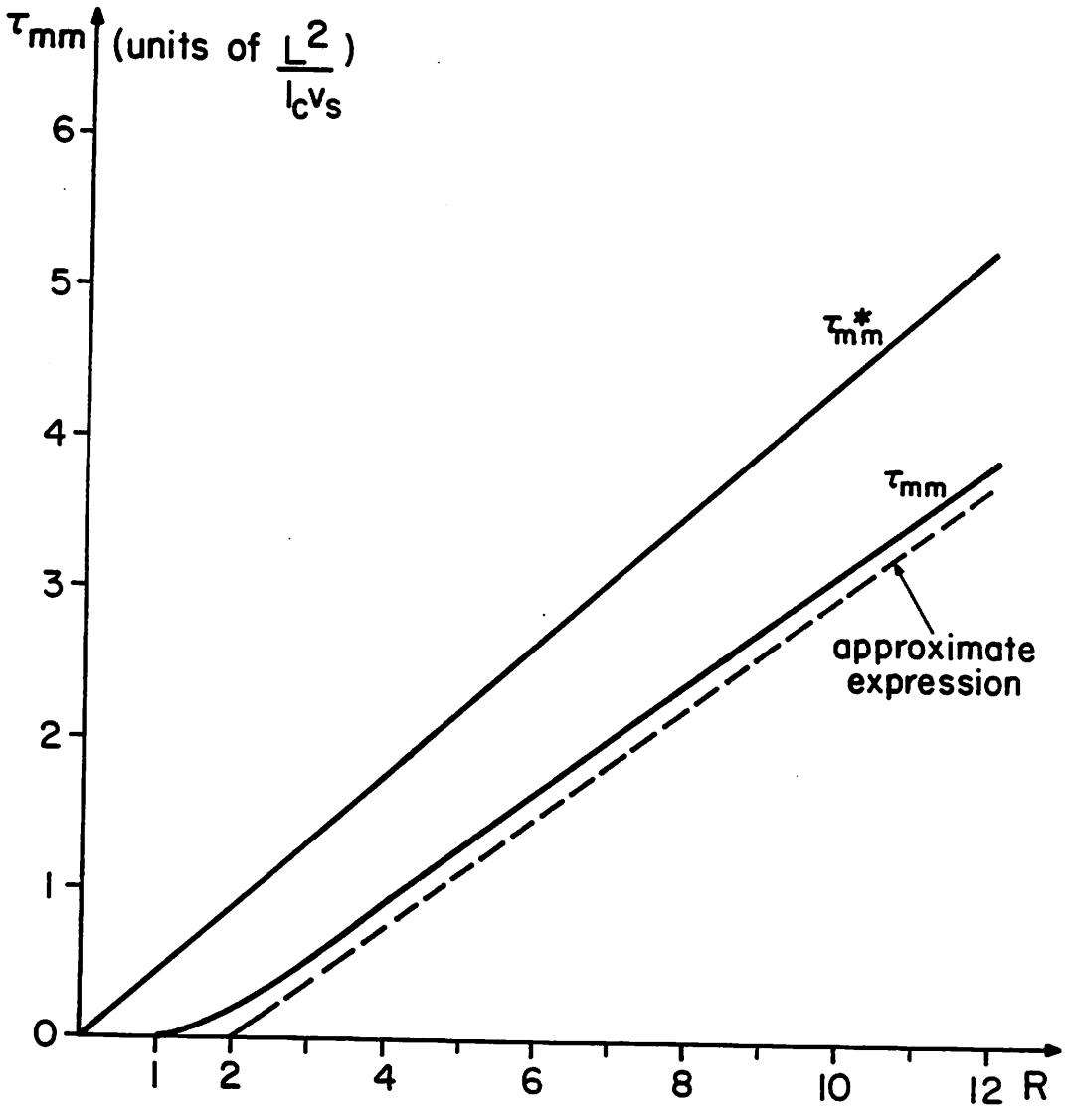
τ_{mm} (units of $\frac{L^2}{l_c v_s}$)
6
5
4
3
2
1
0
τ^*_{mm}
τ_{mm}
approximate expression
1
2
4
6
8
10
12 R

Figure 5.

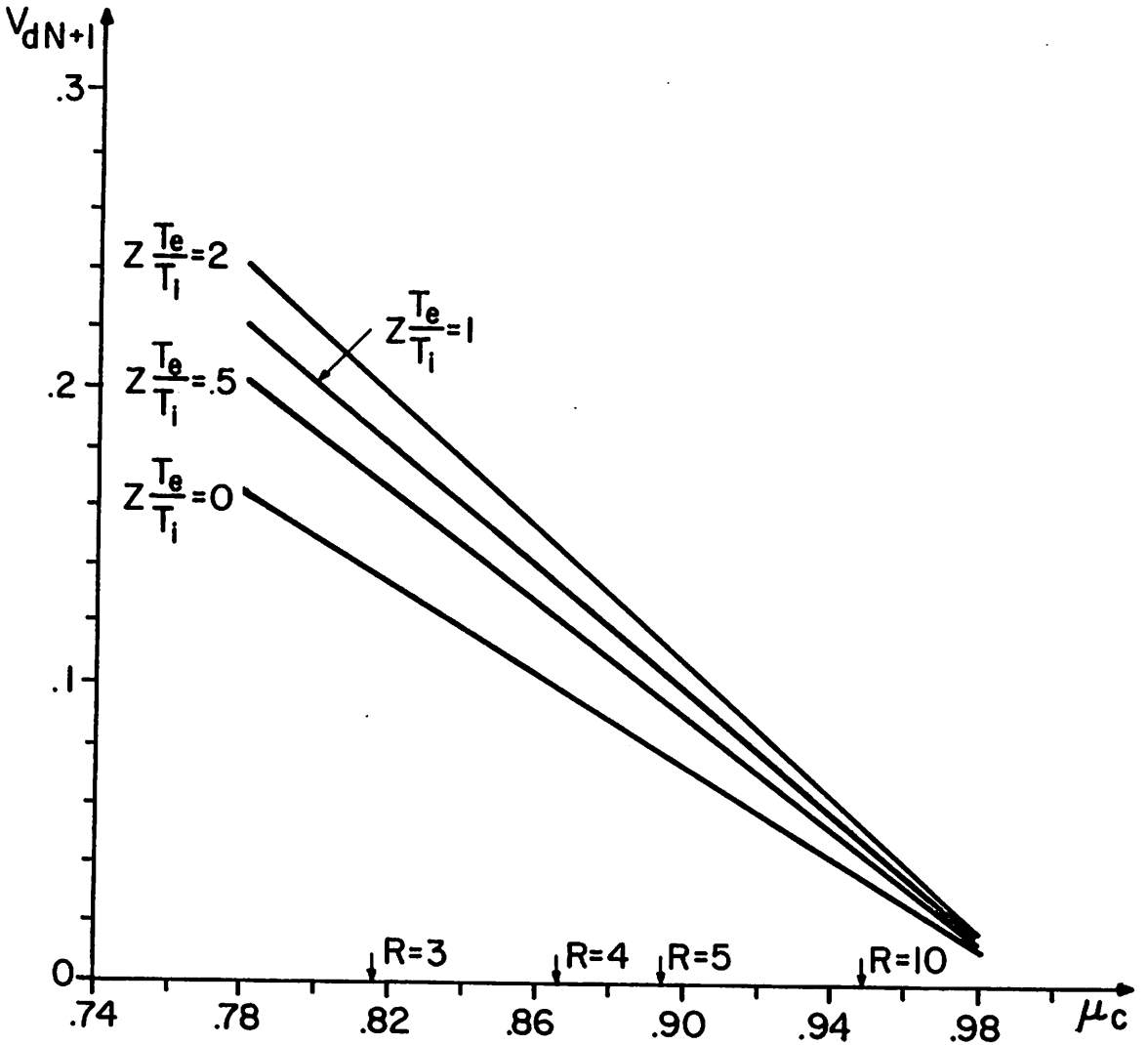
V_{dN+1}
.3
.2
.1
0
$Z\frac{T_e}{T_i}=2$
$Z\frac{T_e}{T_i}=1$
$Z\frac{T_e}{T_i}=.5$
$Z\frac{T_e}{T_i}=0$
R=3
R=4
R=5
R=10
.74
.78
.82
.86
.90
.94
.98
μ_c

Figure 6.

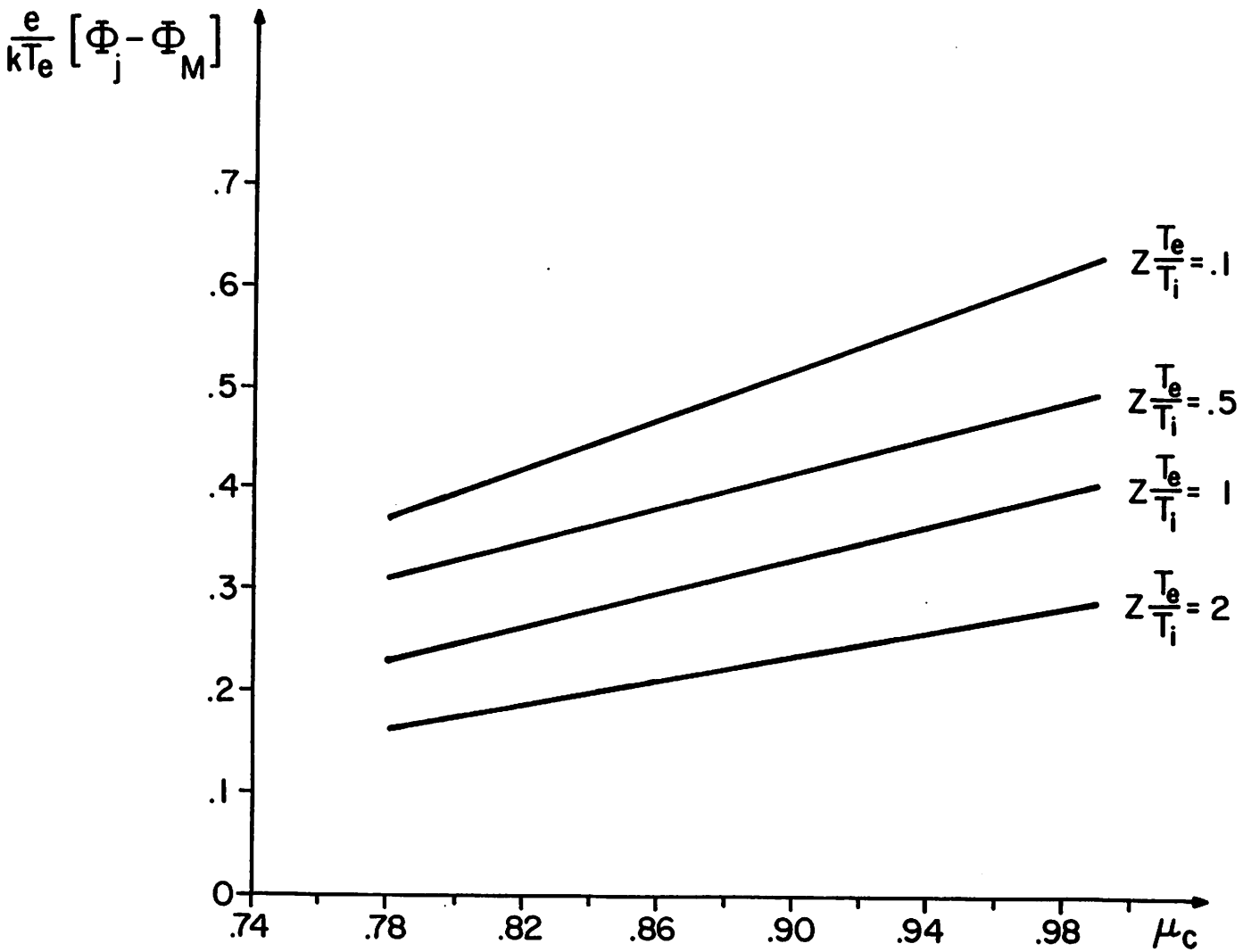
$\frac{e}{kT_e}[\Phi_j - \Phi_M]$
.7
.6
.5
.4
.3
.2
.1
0
.74
.78
.82
.86
.90
.94
.98
μ_c
$Z\frac{T_e}{T_i} = .1$
$Z\frac{T_e}{T_i} = .5$
$Z\frac{T_e}{T_i} = 1$
$Z\frac{T_e}{T_i} = 2$

Figure 7.

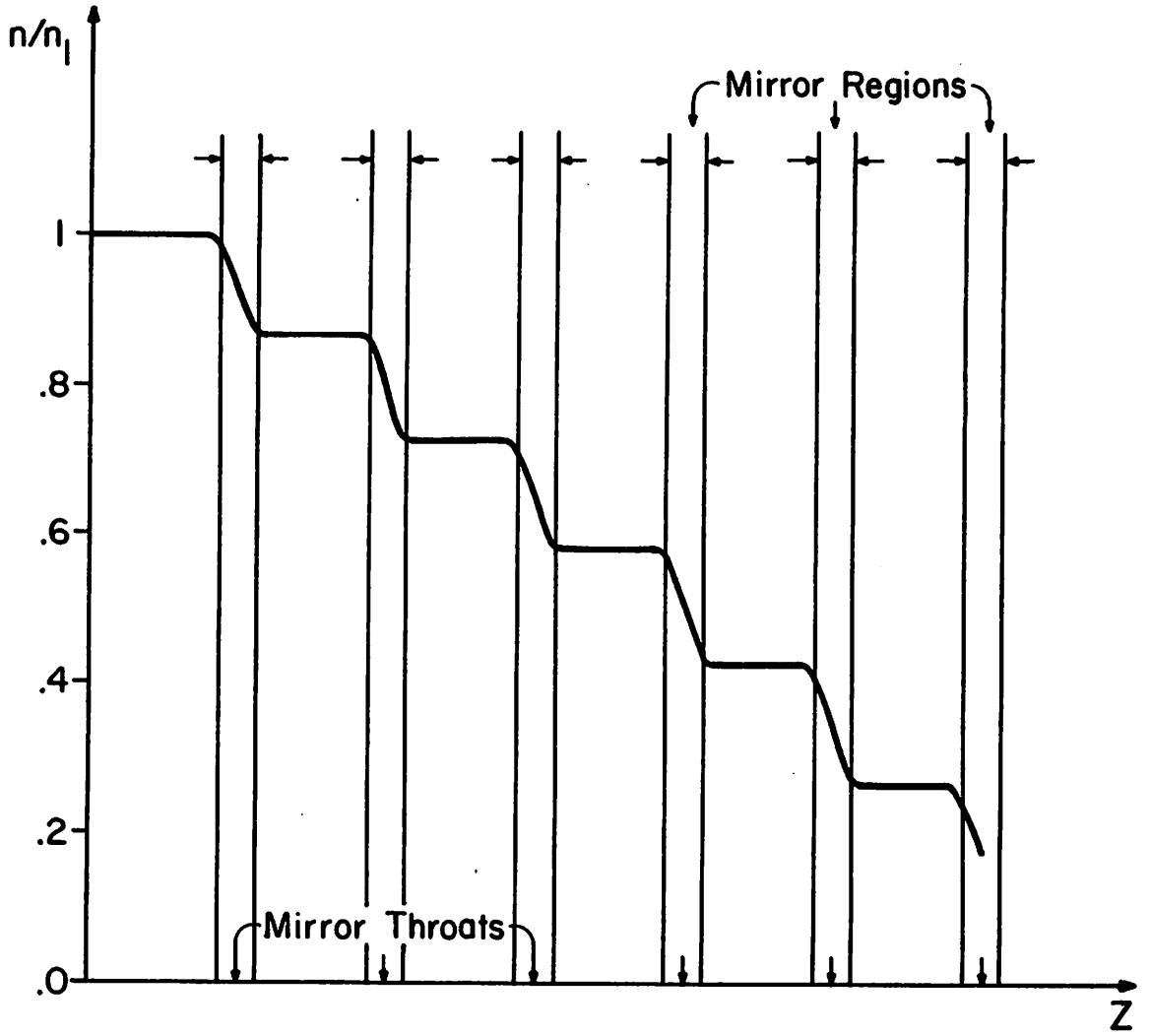

Figure 8a.

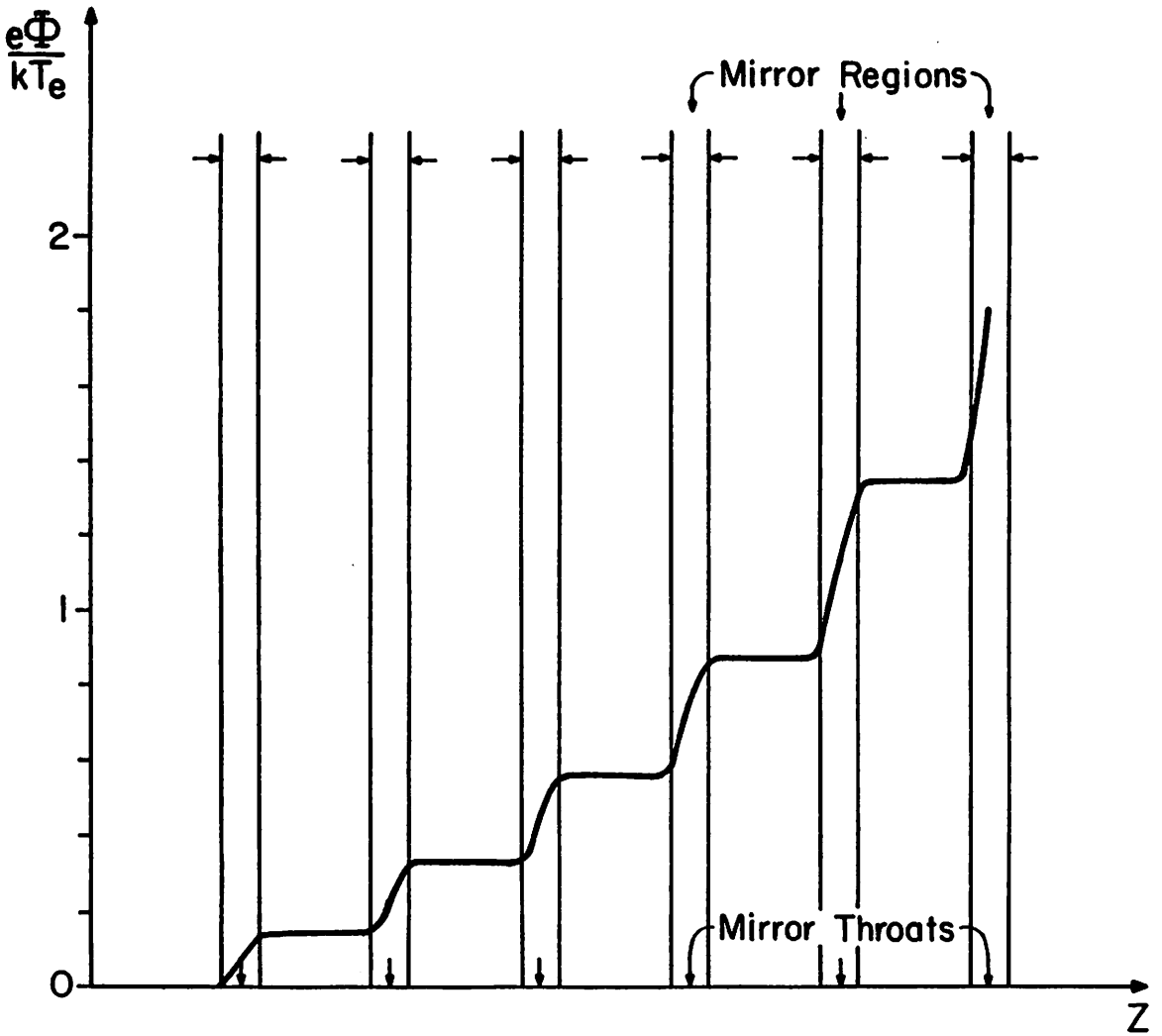

Figure 8b.

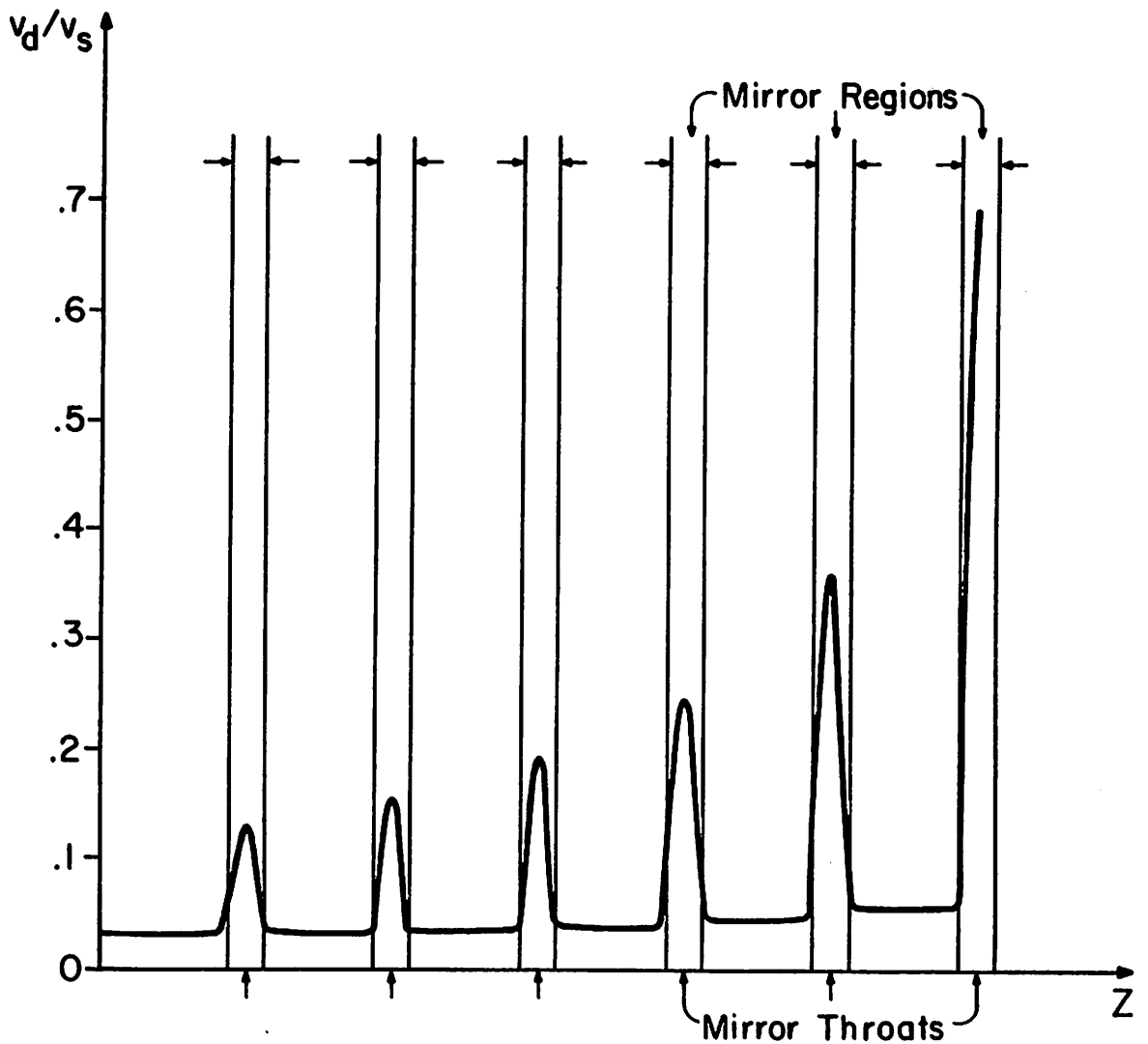

Figure 8c.

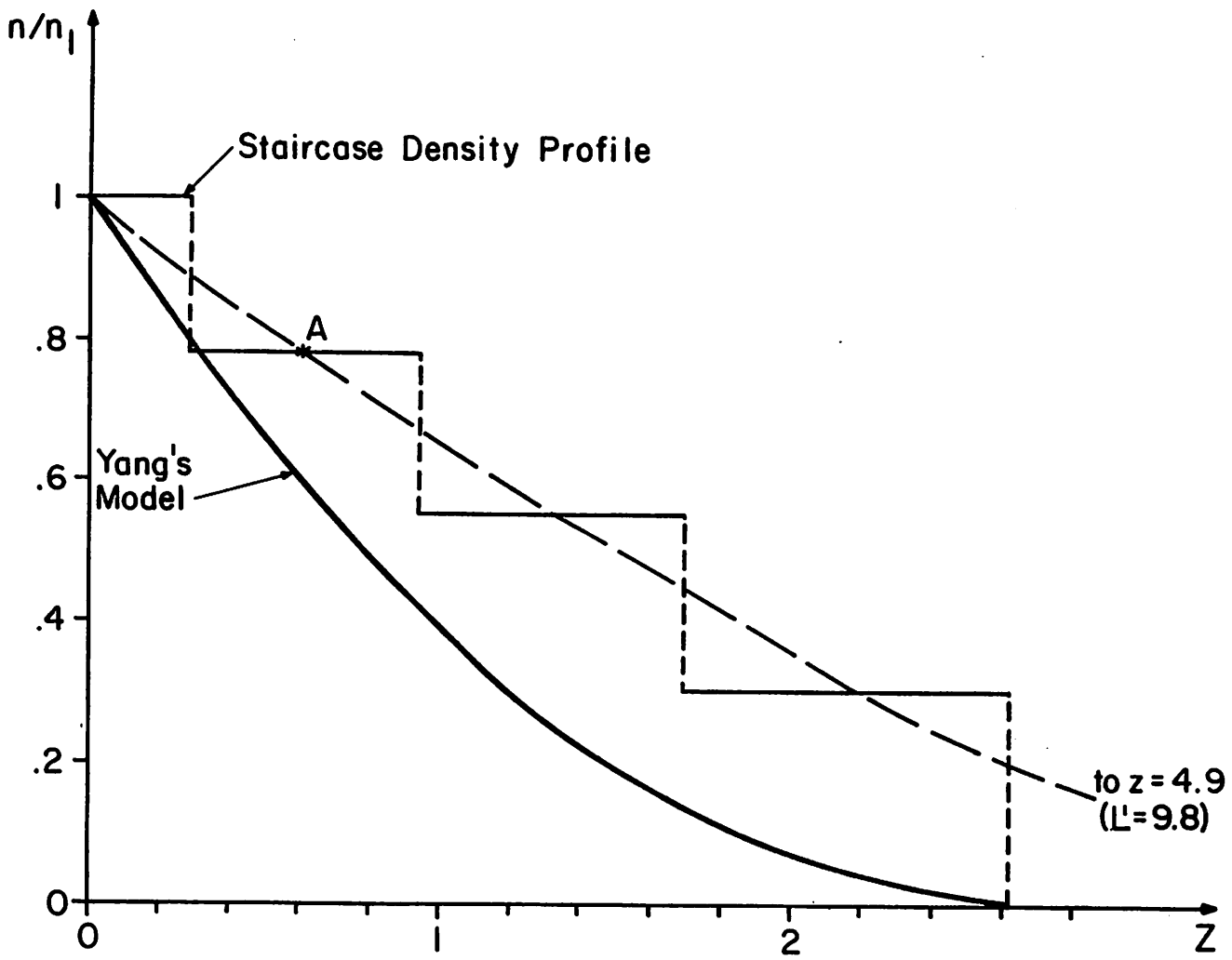
n/n1
Staircase Density Profile
1
.8
.6
.4
.2
0
A
Yang's
Model
to z = 4.9
(L'=9.8)
0
1
2
Z

Figure 9.